Proceedings of ASME Turbo Expo 2011
GT2011
June 6-10, 2011, Vancouver, British Columbia, Canada

GT2011-45722

COUPLED THERMO-MECHANICAL FATIGUE TESTS FOR SIMULATING LOAD CONDITIONS IN COOLED TURBINE PARTS

Roland Mücke and Klaus Rau
Alstom Power
Baden / Switzerland

ABSTRACT

Modern heavy-duty gas turbines operate under hot gas temperatures that are much higher than the temperature capability of nickel superalloys. For that reason, advanced cooling technology is applied for reducing the metal temperature to an acceptable level. Highly cooled components, however, are characterised by large thermal gradients resulting in inhomogeneous temperature fields and complex thermo-mechanical load conditions. In particular, the different rates of stress relaxation due to the different metal temperatures on hot gas and cooling air exposed surfaces lead to load redistributions in cooled structures, which have to be considered in the lifetime prediction methodology. In this context, the paper describes Coupled Thermo-Mechanical Fatigue (CTMF) tests for simultaneously simulating load conditions on hot and cold surfaces of cooled turbine parts, Refs [1, 2]. In contrary to standard Thermo-Mechanical Fatigue (TMF) testing methods, CTMF tests involve the interaction between hot and cold regions of the parts and thus more closely simulates the material behaviour in cooled gas turbine structures. The paper describes the methodology of CTMF tests and their application to typical load conditions in cooled gas turbine parts. Experimental results are compared with numerical predictions showing the advantages of the proposed testing method.

NOMENCLATURE

Symbols

A	cross section area of specimen [m^2]
E	Young's modulus [N/m^2]
T	metal temperature [K]
N	number of load cycle [-]
β^{th}	thermal expansion coefficient [K^{-1}]
ε	total strain [-]
ε^{el}	elastic strain [-]
ε^{in}	inelastic strain [-]
ε^{th}	thermal strain [-]
ε^{mech}	mechanical strain [-]
$\Delta\varepsilon^{th}$	mismatch of thermal strain [-]
$\Delta\varepsilon^{in}$	mismatch of inelastic strain [-]
σ	stress [N/m^2]
CTMF	**C**oupled **T**hermo **M**echanical **F**atigue
TMF	**T**hermo-**M**echanical **F**atigue

Moreover, μ, n, C_1, C_2, β, m, and K denote the material parameters of the Robinson viscoplastic model.

Subscripts

1	sample 1 ("cold" sample)
2	sample 2 ("hot" sample)

Decomposition of strain

Considering small deformations, the total strain ε can be expressed by the additive composition of the thermal strain ε^{th}, the elastic strain $\varepsilon^{el} = \sigma / E$ and the inelastic strain ε^{in},

$$\varepsilon = \varepsilon^{th} + \sigma / E + \varepsilon^{in} \qquad \text{Eq. 1}$$

whereby the inelastic strain contains the viscous (time-dependent) and the plastic (instantaneous) deformation. Further, the elastic strain and the inelastic strain are considered together as mechanical strain

$$\varepsilon^{mech} = \varepsilon^{el} + \varepsilon^{in}, \quad \varepsilon^{mech} = \varepsilon - \varepsilon^{th} \qquad \text{Eq. 2}$$

which results from external forces, temperature gradients and structural constraints. The thermal strain is exclusively produced by the thermal expansion of the material.

INTRODUCTION

Advances in the lifetime prediction methods of hot gas exposed components of heavy-duty gas turbines can be related either to improvements in the computational models for simulating the constitutive and the lifing behaviour of advanced turbine materials or to improvements in the material testing methods considering realistic load conditions. While specific enhancements of the computational models for heavy-duty gas turbine parts have been discussed in Refs [3-6], this paper is addressing an improved testing methodology for high temperature materials and its application to typical gas turbine load conditions. In this context, so-called **C**oupled **T**hermo-**M**echanical **F**atigue (CTMF) tests are described, which allow the simultaneous simulation of the load conditions in hot and cold regions of the component. In contrast to standard **T**hermo-**M**echanical **F**atigue (TMF) tests, which consider the material points independent on each other, CTMF tests take into account the interaction between different regions of the structure.

The paper describes the application of CTMF tests to gas turbine materials. Pairs of two specimens are applied to simultaneously simulate hot and cold volume elements in a cooled structure as typical for leading edges of turbine blades or other structures with large thermal gradients. The development of the stress-strain hysteresis and the respective cyclic deformation curves resulting from different external loadings are discussed. Finally, a comparison of the experimental results with numerical predictions is shown.

LOAD CONDITIONS IN COOLED GAS TURBINE PARTS

Load conditions of hot gas exposed components in heavy duty gas turbines are complex for different reasons: First, the engine operation concept (engine start / stop procedures, full load / part load operation, fuel switch over, frequency response) results in specific time histories of metal temperatures and mechanical loading due to time variations in the thermal boundary conditions as well as transient effects. Second, advanced cooling technology causes inhomogeneous temperature fields and, in particular, large temperature gradients within cooled walls, Refs [7, 8]. As an example, Figure 1 shows the temperature distribution in a cooled turbine blade around the leading edge. Note that the loading in each of the material points depends on the specific ratio of force and displacement controlled load conditions. Thereby, the force controlled loading is driven by centrifugal load and gas pressure while the displacement controlled load conditions are caused by the thermal mismatch between the average thermal expansion of the blade airfoil and the considered material point. In stationary gas turbines rotating with grid frequency, the thermal load predominates the centrifugal and pressure load. Under this condition, the hot gas exposed surface at the leading edge of a turbine blade (Point A in Figure 1) – which is

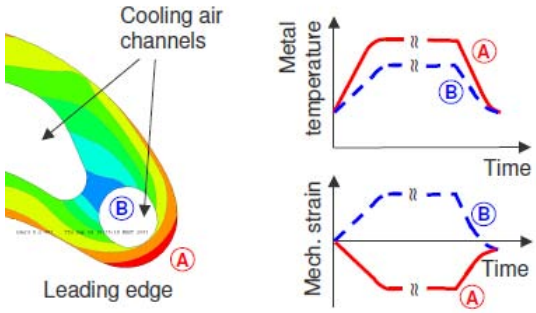

Figure 1: Example of temperature distribution and schematic load history in cooled turbine blades.

typically hotter than the average metal temperature in the airfoil section – undergoes compression since the thermal expansion is constrained by the colder regions. On the other hand, the web region between two cooling channels (Point B in Figure 1) experiences a tension under engine operation condition since it is constrained by the higher average temperature of the airfoil section. Moreover, the different stationary temperature levels cause different loading rates in hot and cold parts of the structure.

STANDARD LOAD CYCLES FOR MATERIAL TESTING

For cyclic life prediction of hot gas exposed components, the specific load cycles of each material point are related either to

- strain-controlled isothermal fatigue load cycles,
- standardized **O**ut-of-**P**hase **T**hermo-**M**echanical **F**atigue load cycles (OP TMF), or
- **I**n-**P**hase **T**hermo-**M**echanical **F**atigue load cycles (IP TMF).

OP TMF load cycles are characterized by a decreasing mechanical strain while the temperature increases,

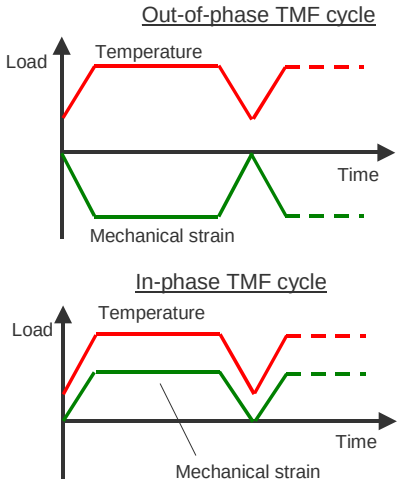

Figure 2: Out-of-Phase and In-Phase TMF cycles.

whereas in IP TMF cycles both mechanical strain and temperature are increasing, Figure 2. OP TMF cycles typically occur on hot gas exposed surfaces of cooled turbine parts, whereas IP TMF cycles often (but not exclusively) arise on coolant air exposed surfaces.

"Conventional" low cycle isothermal fatigue and thermo-mechanical fatigue tests ignore the interaction between "hot" and "cold" parts of cooled components. This interaction results in a load redistribution, which is driven by the following phenomena:

- Due to different metal temperatures in hot and cold regions there are significantly different rates of stress relaxation in the component.
- The rates of temperature during heating and cooling phases are different in hot and cold regions.
- The temperature dependencies of Young's modulus and yield strength result in different material stiffness's in hot and cold regions.

COUPLED THERMO-MECHANICAL FATIGUE TESTS

The above listed complex interaction phenomena between hot and cold regions of cooled turbine components can be analysed by "**C**oupled **T**hermo-**M**echanical **F**atigue" (CTMF) tests. In CTMF tests two or more samples are simultaneously tested. Thereby, each sample is mounted in a separate load frame so that every sample can undergo individual temperature-time and loading-time paths. Their mutual constraints are realized by keeping the total strains of the investigated specimens at identical values. The simulation of external forces is possible by applying a loading as the sum of the forces F_S on both specimens.

We now consider an arrangement with two TMF testing systems, Figure 3. In this case, the following four boundary conditions are realized by closed-loop control circuits:

- Separate temperature-time paths for both specimens

$$T_1 = T_1(t) \qquad \text{Eq. 3}$$

$$T_2 = T_2(t) \qquad \text{Eq. 4}$$

- Independent time path for the sum of forces

$$F_1(t) + F_2(t) = F_S(t) \qquad \text{Eq. 5}$$

- Equal total strains at both specimens at every point of time

$$\varepsilon_1(t) = \varepsilon_2(t) \qquad \text{Eq. 6}$$

The equilibrium of forces, Eq. 5, and the condition of compatibility, Eq. 6, as well as the decomposition of strain

$$\varepsilon_1 = \varepsilon_1^{th} + \sigma_1 / E_1 + \varepsilon_1^{in} \qquad \text{Eq. 7}$$

$$\varepsilon_2 = \varepsilon_2^{th} + \sigma_2 / E_2 + \varepsilon_2^{in} \qquad \text{Eq. 8}$$

give the following system of equations

$$\sigma_1 A_1 + \sigma_2 A_2 = F_S \qquad \text{Eq. 9}$$

$$\Delta\varepsilon^{th} + \Delta\varepsilon^{in} + \sigma_2 / E_2 - \sigma_1 / E_1 = 0 \qquad \text{Eq. 10}$$

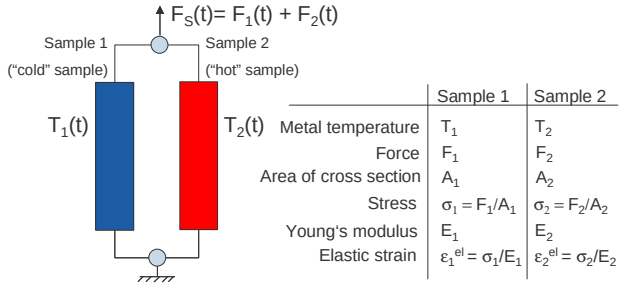

Figure 3: Sketch of CTMF tests with two specimens.

where $\Delta\varepsilon^{th} = \varepsilon_2^{th} - \varepsilon_1^{th}$ and $\Delta\varepsilon^{in} = \varepsilon_2^{in} - \varepsilon_1^{in}$ denote the thermal mismatch and the difference in inelastic strain between sample 1 and sample 2, respectively, E_1, E_2 describes the Young's modulus and A_1, A_2 name the cross section area of specimen 1 and 2. Note that due to the temperature dependence of the Young's modulus, the stiffness of the specimens is different even when the same material is applied for both samples.

Using Eqs 7 to 10, the following analytical expressions are obtained for the stresses and the total strain:

$$\sigma_1 = E_1\left(\frac{F_S}{E_1A_1 + E_2A_2} + \frac{\Delta\varepsilon^{th} + \Delta\varepsilon^{in}}{1 + E_1A_1/(E_2A_2)}\right) \qquad \text{Eq. 11}$$

$$\sigma_2 = E_2\left(\frac{F_S}{E_1A_1 + E_2A_2} - \frac{\Delta\varepsilon^{th} + \Delta\varepsilon^{in}}{1 + E_2A_2/(E_1A_1)}\right) \qquad \text{Eq. 12}$$

$$\varepsilon = \frac{F_S}{E_1A_1 + E_2A_2} + \frac{E_1A_1(\varepsilon_1^{th} + \varepsilon_1^{in}) + E_2A_2(\varepsilon_2^{th} + \varepsilon_2^{in})}{E_1A_1 + E_2A_2} \qquad \text{Eq. 13}$$

Above equations are valid for general constitutive behaviour and for small strains, i.e. the strain composition holds and the changes of the cross section areas A_1 and A_2 are neglected. The case of elastic material behaviour is obtained from the general equations by setting $\varepsilon_2^{in} = \varepsilon_1^{in} = 0$ and $\Delta\varepsilon^{in} = 0$. Note that above equations allow the following interpretation:

- The stresses in the specimens depend on the sum of external forces as well as the *mismatch* of thermal and inelastic strains.
- The total strain depends on the sum of external forces as well as the *stiffness-weighted average* of thermal and inelastic strain.
- The stresses σ_1 and σ_2 are equal when using the same material and temperature for both specimens, i.e. $\Delta\varepsilon^{th} = 0$ and $\Delta\varepsilon^{in} = 0$.
- The stresses are equal but have opposite sign ($\sigma_1 = -\sigma_2$) for zero sums of external forces ($F_S = 0$) and equal cross section areas ($A_1 = A_2$).

EXPERIMENTAL DETAILS

The thermo-mechanical tests were carried out on pairs of standard cyclic test specimens of the nickel superalloy MarM247. The CTMF tests were performed on two cyclic testing facilities which mainly consists of two servo-hydraulic load frames with a nominal force capacity of 100 kN each, two inductive furnaces and a four-channel MTS TestStar device for controlling the complete system, Refs [1, 2].

Before starting the test, the thermal strains ε_1^{th} and ε_2^{th} are measured as function of T_1 and T_2. During the test, the cycle number (N), the external forces (F_1, F_2), the total strains ($\varepsilon_1 = \varepsilon_2$) and the temperatures ($T_1$, T_2) of both specimens are stored as function of time. The mechanical strain is calculated by subtracting the thermal strain from the total strain, $\varepsilon^{mech} = \varepsilon - \varepsilon^{th}$. The stress is evaluated by dividing the applied force by the area of the cross section, $\sigma = F / A$. Thus for each specimen the σ - ε^{mech} hysteresis as well as the cyclic deformation curves (maximum and minimum stress and strain of the cycle versus the cycle number) are determined.

All tests are carried out with equal temperature-time paths with a minimum temperature of $T_{min} = T_{1,min} = T_{2,min}$ = 50°C and maximum temperatures of $T_{1,max}$ and $T_{2,max}$ corresponding to specific temperature conditions on the cooling air side and the hot gas side of cooled turbine parts, Figure 4. The time period of each cycle is 1000 s including a dwell time at maximum temperature of 600 s. The external forces are simulated by force-time paths, which are proportional to the temperature of both specimens with a phase shift of 180°. The forces have maximum values corresponding to stresses of 0 MPa, -200 MPa and –350 MPa, respectively. The tests have been completed, when one of the specimens showed a load drop of 2%.

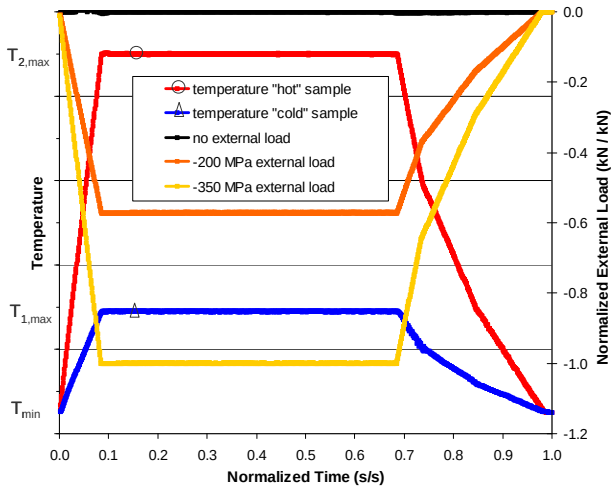

Figure 4: Temperatures and external forces versus time.

RESULTS OF CTMF TESTS

In Figure 5, the total strain ε, the thermal strain ε^{th}, and the mechanical strain ε^{mech} of sample 1 (cold) and sample 2 (hot) are plotted versus time for the first cycle. According to Eq. 6, the total strains are identical in both samples at all time, and, consequently, the relationship $\varepsilon_1^{th} < \varepsilon < \varepsilon_2^{th}$ holds during heating up. Because of the lower heating rate in the "cold" sample (sample 1), the thermal strain in the "hot" sample (sample 2) is partially constrained. This results in a mechanical strain-time course ε_2^{mech}, which is about 180° phase shifted to the respective thermal strain-time path. In contrast, ε_1^{mech} ("cold" sample) is nearly in phase with ε_1^{th}.

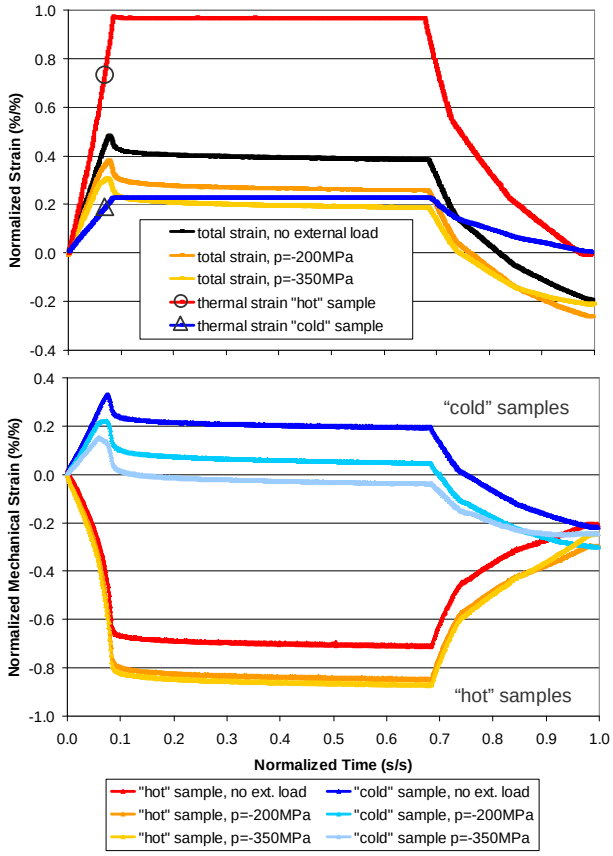

Figure 5: Measured total, thermal and mechanical strain in the first load cycle.

CTMF behaviour at F_S = 0. While heating the "cold" sample with a smaller heating rate than the "hot" sample, a compressive stress σ_2 occurs in the "hot" sample which reaches its maximum value about 15 s before the maximum temperature, Figure 6. During the same time, the mechanical strain ε_2^{mech} approaches only about 2/3 of the value at maximum temperature $T_{2,max}$. The effect of the decreasing stress after reaching the maximum while the mechanical strain is increasing ("dynamic relaxation") is related to the decreasing Young's modulus and the

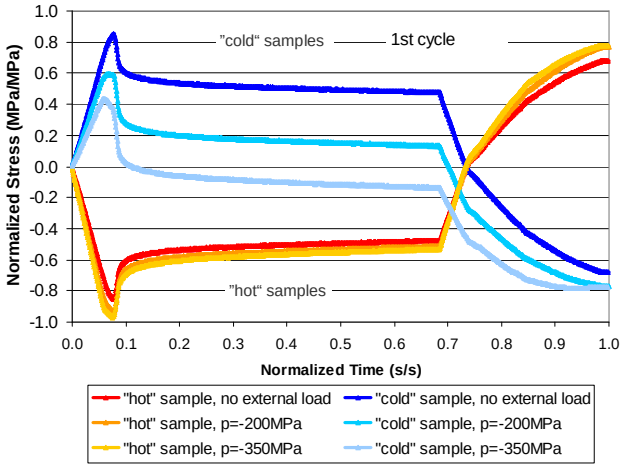

Figure 6: Measured stress versus time in the first load cycle.

decreasing material flow resistance at higher temperature. During the dwell time the compressive mechanical strain slightly increases while the compressive stress decreases due to inelastic relaxation processes. During unloading, the compressive stress decreases considerably and changes to tensile stress after about 730s at about 640°C. For the case without external loading, the relationship $F_1(t) + F_2(t) = F_S(t) = 0$ holds which corresponds to $\sigma_1 = -\sigma_2$ at every point of time. The residual negative total strain and the residual stresses in both samples after the first cycle indicate extensive plastic deformation which results in an open hysteresis in the strain-stress diagram, Figure 7. As shown in Figure 7a, high compressive plastic deformation, caused by high mechanical loading at high temperatures, occurs in the "hot" sample in the first cycle (N = 1). In the "cold" sample only small tensile plastic deformations occur because the mechanical loading ε_1^{mech} is acting at significantly lower temperature. At the end of the cycle at minimum temperature $T_{1,min} = T_{2,min} = 50°C$, the thermal strains ε_1^{th} and ε_2^{th} are zero and therefore the total strain equals the mechanical strains $\varepsilon(T_{min}) = \varepsilon_1^{mech} = \varepsilon_2^{mech}$. The residual (total) strain at the end of the first cycle reaches $\varepsilon(T_{min}) \approx -0.27\%$ which means that the system consisting of both samples has shortened during the cycle. The further development of the hysteresis in cycle N = 2 and N = 100 is shown in Figure 7b and Figure 7c. The plastic deformations of the "hot" samples have considerably decreased in the second cycle and further decreased in cycle N=100. The "cold" sample shows elastic behaviour from N = 2. During the same time, the stress range $\Delta\sigma = \sigma_{max} - \sigma_{min}$ slowly decreases.

The development of the maximum and minimum values of the stresses of each cycle is shown in Figure 8. As mentioned above, the relations $F_1(t) + F_2(t) = F_S(t) = 0$ and $\sigma_1 = -\sigma_2$ hold for the case without external load. This implies that the minimum stress in sample 1 is identical with the maximum stress in sample 2 and vice versa, i.e. $\sigma_{1,min} = -\sigma_{2,max}$.

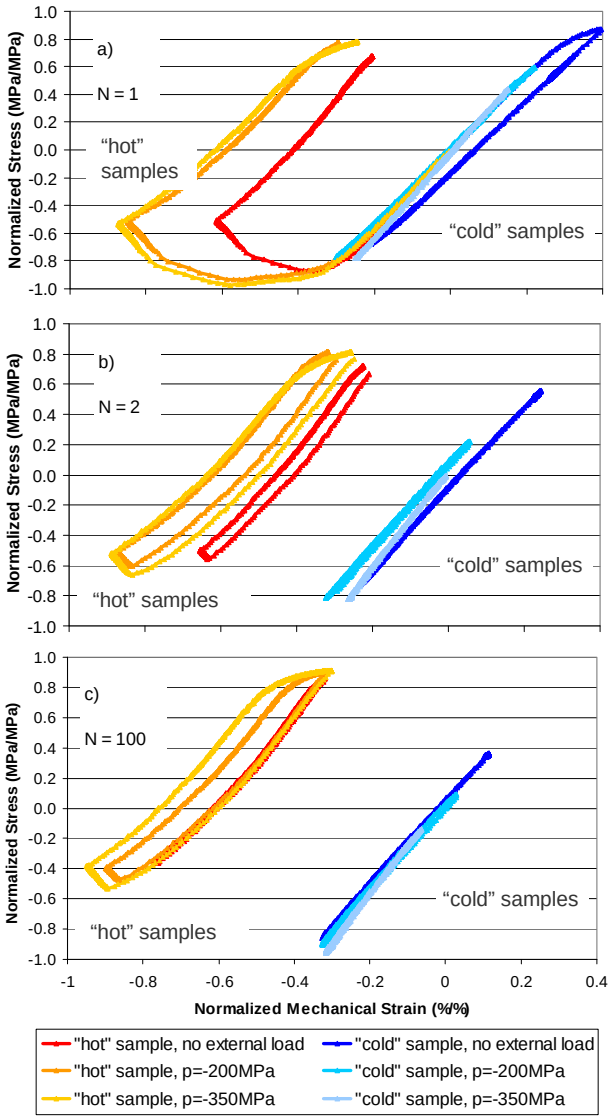

Figure 7: Measured hysteresis of stress versus mechanical strain in the first (a), the second (b) and the 100th (c) load cycle.

During the first 50 cycles, the maximum and minimum values of the stresses are increasing in the "hot" sample and decreasing in the "cold" sample. After the first 50 cycles, the maximum and minimum values remain about constant until the crack initiation leads to a drop of the absolute values. The maximum and minimum values of the total strain in Figure 8 show decreasing values, which indicates cyclic creep toward negative strain especially during the first 50 cycles.

CTMF behaviour at $F_S = F_1 + F_2 \neq 0$: As shown in Figure 5 and Figure 6, external compressive loadings result in a shift of the total strain, the mechanical strain and the stress of both samples towards lower values during heating and dwell whereas the residual stresses of the

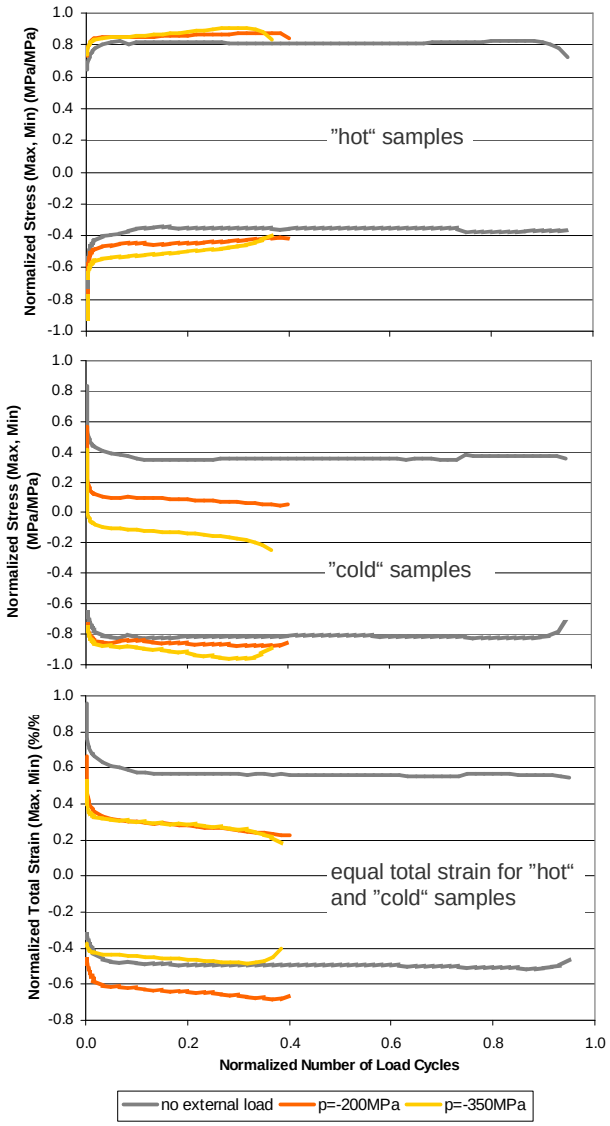

Figure 8: Measured maximum and minimum stress and total strain versus number of load cycle.

"hot" samples are higher for higher external compressive loadings. In particular:

- In the "cold" sample the shift in the stress is driven by the external compressive loading. In the "hot" sample the stresses are nearly the same for p=-200MPa and p=-350MPa because the dynamic relaxation at high temperature prevents a further stress built up, Figure 6.
- Increasing absolute values of the external load result in increasing plastic deformations, Figure 7, as well as higher tensile and compressive stresses in the "hot" sample, Figure 8.
- In the "cold" sample, no plastic deformation occurs for the cases with external load (closed hysteresis loops in Figure 7), however, the minimum and maximum stress decreases, Figure 8, because of plasticity in the "hot" sample.
- The stress range $\Delta\sigma = \sigma_{max} - \sigma_{min}$ for the "hot" sample increases with increasing absolute values of $F_{S,max}$ whereas it decreases for the "cold" sample, Figure 8.

NUMERICAL RESULTS

The Robinson viscoplastic model. The numerical simulations are based on the Robinson unified viscoplastic model. Different variants of this model are reported in Refs [9-11]. The constitutive equations applied in this work are summarized in Table 1. Apart from the definitions given there, G_0 is a cut-off parameter which prevents the rate of the back stress X from becoming singular for small G, T_0 describes a reference temperature associated with zero thermal strain, and the symbol $\langle . \rangle$ denotes the Macauley bracket

$$\langle x \rangle = \begin{cases} x & \text{for} \quad x \geq 0 \\ 0 & \text{for} \quad x < 0 \end{cases} \qquad \text{Eq. 14}$$

Table 1: Governing equations of the Robinson model.

a) Strain decomposition:	$\varepsilon = \varepsilon^{th} + \varepsilon^{mech}$ with $\varepsilon^{mech} = \varepsilon^{el} + \varepsilon^{in}$
b) Thermal strain:	$\varepsilon^{th} = \beta^{th}(T)\,(T - T_0)$
c) Elastic strain:	$\varepsilon^{el} = \sigma / E$
d) Flow rule:	$\dot{\varepsilon}^{in} = Fd \quad \text{for} \quad \sigma(\sigma - X) > 0$
e) Flow function:	$F = \frac{1}{2\mu}\left\langle \frac{(\sigma - X)^2}{3K^2} - 1 \right\rangle^n$
f) Flow direction:	$d = \text{sgn}(\sigma - X)$
g) Rate of back stress:	$\dot{X} = \frac{3}{2} C_1 G^{-\beta} \dot{\varepsilon}_{in} - \sqrt{3} C_2 G^{-m} \text{sgn}(X)$ with $G = \begin{cases} X^2/3K^2 & \text{for} \quad X^2/3K^2 \geq G_0 \\ G_0 & \text{for} \quad X^2/3K^2 < G_0 \end{cases}$
h) Material parameters:	$\mathbf{P}_{el} = [E, \beta^{th}]$ $\mathbf{P}_{in} = [\mu, n, C_1, C_2, \beta, m, K]$

Remarks:

1. The equations in Table 1 describe the uniaxial formulation of the Robinson model in load direction since this is sufficient for the simulation of the CTMF tests. The corresponding multiaxial equations required for component scale simulations can be found in Ref [12].
2. Modeling large temperature ranges requires the temperature dependence of the material parameters to be taken into account. For doing so, the material parameters were determined at different temperature levels and suitable interpolation schemes for intermediate temperatures have been applied. The material parameters of the Robinson model were determined separately from the CTMF tests.

3. Temperature rate terms for the hardening parameters C_1 and β are applied for the simulation of large temperature ranges and fast transients.

Note that the multiaxial Robinson model including the development of temperature rate terms and details on the identification of material parameters have been reported in Ref [12].

Results of simulation. Results of the computational simulations of the CTMF tests are shown in Figure 9. Note that the stress redistribution is well predicted by the numerical model. In particular, the numerical model computes a stress relaxation in the "hot" sample. Because of the equilibrium of force, the stress in the "cold" sample changes accordingly. This effect would not be observed in standard TMF tests since under cold conditions no pronounced stress relaxation takes place. Note further that the external force mainly influences the stress in the cold

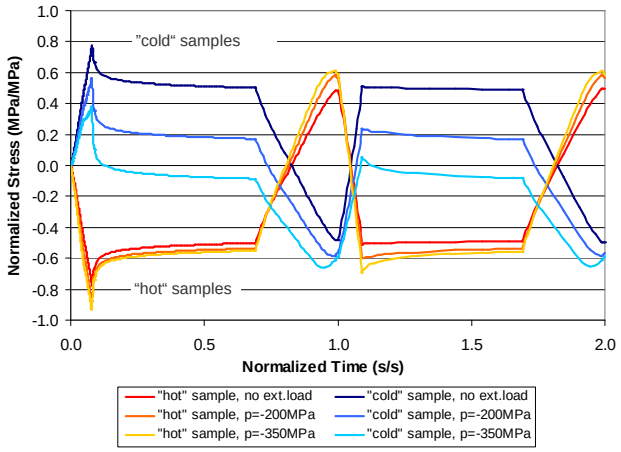

Figure 9: Predicted stress in the first two load cycles.

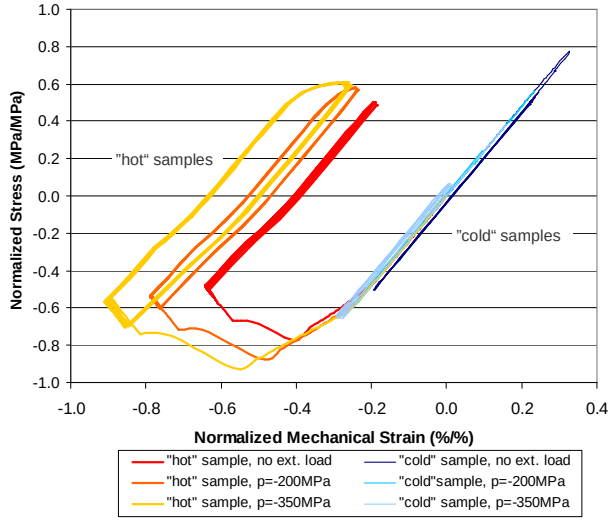

Figure 10: Predicted stress versus mechanical strain.

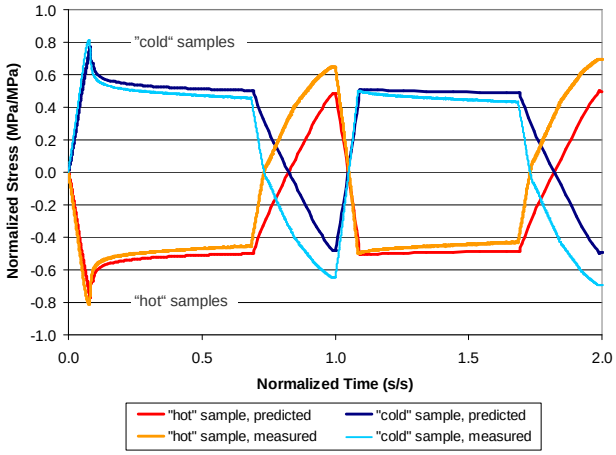

Figure 11: Comparison of measured and predicted stress cycles for zero external force.

sample, as also seen in the measurements, whereas the stresses in the hot sample are nearly independent on external forces.

The stress versus mechanical strain in the first 5 cycles is shown in Figure 10. Note that, as in the experimental data, the external force of 350MPa produces a significant hysteresis in the hot sample whereas in the cold sample the cycles are nearly elastic.

Finally, Figure 11 combines measurements and computational predictions for the case of zero external load. Note that the stresses during heating up and dwell time are well predicted while during shut down the experimental data show a more pronounced stress rise. This can be related to the temperature history, which in the tests is realized by convective heat transfer, while in the simulation a simple ramp down function has been applied for the temperature.

CONCLUDING REMARKS

The paper describes Coupled Thermo-Mechanical Fatigue (CTMF) tests for simulating the interaction of hot and cold regions of cooled gas turbine components. Compared to standard TMF fatigue testing, CTMF tests offer the following advantages:

- CTMF tests are not restricted to the simulation of the local behaviour of the materials (in the sense of the local concept to cyclic life prediction) because they take the stress redistribution - in particular between hot and cold regions of cooled component - into account.
- Thermo-mechanical load conditions with complex phase relations between temperature and mechanical loadings can be simulated, as it occurs in transient situations where the mechanical load approaches its maximum before the temperature reaches the stationary level.
- Different material combinations and their interaction can be tested, e.g. base metal / coating systems.

- CTMF tests can be applied for checking the capability of viscoplastic constitutive models since they involve a wide range of deformation mechanisms.

In this context, CTMF tests improve the understanding of the material behaviour under complex load conditions as they occur in cooled parts of gas turbine engines.

REFERENCES

[1] T. Beck, K.-H. Lang, O. Vöhringer, D. Löhe, Experimental analysis of the interaction of hot and cold volume elements during thermal fatigue of cooled components made from AISI 316 L steel, Zeitschrift für Metallkunde, Vol. 92, 08/2001, 875-881.

[2] K. Rau, T. Beck, D. Löhe, Isothermal thermo-mechanical and complex thermo-mechanical fatigue tests on AISI 316 L steel – a critical evaluation, Material Science and Engineering A345 (2003), 309-318.

[3] R. Mücke, A viscoplastic modelling approach for MCrAlY protective coatings for gas turbine applications, ASME Journal for Gas Turbines and Power, November 2009, Vol 131 / Issue 6 (and Proceedings of ASME Turbo Expo 2008, paper No. GT2008-50579).

[4] R. Mücke, O.-E. Bernhardi, A Constitutive Model for Anisotropic Materials based on NEUBER'S Rule, Computer Methods in Applied Mechanics and Engineering 192 (2003) 4237-4255.

[5] R. Mücke, P. Woratat, A cyclic life prediction approach for directionally solidified nickel superalloys, ASME Journal for Gas Turbines and Power, May 2010, Vol. 132, Issue 5 (and Proceedings of ASME Turbo Expo 2009, paper No. GT2009-59180).

[6] W. D. Day, Modified Morrow mean stress correction of Manson-Coffin life prediction models, Proceedings of ASME Turbo Expo 2011, paper No. GT2011-45444.

[7] J. Krückels, T. Arzel, T. R. Kingston, M. Schnieder, Turbine blade thermal design process enhancements for increased firing temperatures and reduced coolant flow, Proceedings of ASME Turbo Expo 2007, paper No. GT2007-27457.

[8] J. Krückels, W. Colban, M. Gritsch, M. Schnieder, Validation of a first vane platform cooling design for a high lift profile application, Proceedings of ASME Turbo Expo 2011, paper No. GT2011-45252.

[9] D. N. Robinson, Constitutive relationships for anisotropic high-temperature alloys, Nuclear Engineering and Design 83 (1984) 389-396.

[10] D. N. Robinson, A unified creep-plasticity model for structural metals at high temperatures, ORNL Report TM-5969 (1978), Oak Ridge National Laboratory.

[11] D. N. Robinson, P. A. Bartolotta (1985), Viscoplastic constitutive relationships with dependence on thermo-mechanical history, NASA report CR-174836 (1985).

[12] R. Mücke, O. E. Bernhardi, On temperature rate terms for viscoplastic constitutive models with applications to high temperature materials, Comput. Methods Appl. Mech. Engrg. 195 (2006) 2411-2431.